PFC/JA-92-27

Spatiotemporal Chaos In Three Wave Interactions

C. C. Chow, A. Bers, and A. K. Ram

September 1992

Plasma Fusion Center
Massachusetts Institute of Technology
Cambridge, MA 02139 USA

This work was supported in part by NSF Grant No. ECS-88-22475, NASA Grant No. NAGW-2048, DOE Grant No. DE-FG02-91ER-54109, and LLNL subcontract B160456.

To appear in: *Plasma Physics and Controlled Fusion*, **Special Issue**: Invited Papers for the 1992 ICPP, Innsbruck, Austria, 29 June -- 3 July 1992.

SPATIOTEMPORAL CHAOS IN THREE WAVE INTERACTIONS

C. C. Chow, A. Bers, and A. K. Ram

SPATIOTEMPORAL CHAOS IN THREE WAVE INTERACTIONS

C. C. CHOW, A. BERS AND A. K. RAM

Plasma Fusion Center and Research Laboratory of Electronics
Massachusetts Institute of Technology, Cambridge, MA 02139 USA

ABSTRACT

It is shown that the saturated state of an unstable wave nonlinearly coupled to two lower frequency damped waves exhibits spatiotemporal chaos. The results can be understood by perturbation analysis on the conservative nonlinear three-wave interaction which is integrable.

KEYWORDS

Nonlinear wave interactions; unstable wave saturation; chaos in space-time

INTRODUCTION

The nonlinear three wave interaction (3WI) in spacetime has numerous applications to plasma physics (Bers, 1975; Kaup *et al.*, 1979). The linear evolution of this interaction describes parametric instabilities, both absolute and convective, as well as the stable coupling of waves. We consider the case of the nonlinear saturation of a linearly unstable parent wave by coupling to two damped daughter waves (Chow, 1991; Chow *et al.*, 1992a; Chow *et al.*, 1992b) This system exhibits spatiotemporal chaos (STC). The term STC specifically refers to the chaotic dynamics of coherent structures or spatial patterns (Hohenberg and Shraiman, 1989; Coullet *et al.*, 1987; Arrechi *et al.*, 1990; Ciliberto and Caponeri, 1990). This is contrasted with fully developed turbulence where there is a cascade to small scales, and is different from low dimensional chaos where spatial degrees of freedom are not involved. The conservative form of the 3WI is integrable by inverse scattering transforms (IST) and may have soliton solutions (Kaup *et al.*, 1979; Kaup, 1976a; Zakharov and Manakov, 1973). We consider the nearly integrable limit of the 3WI and use numerical simulations and perturbation theory about the IST solutions to gain some understanding of the dynamics.

The 3WI is a ubiquitous interaction that can occur whenever three linear waves are in resonance in a weakly nonlinear medium (Benney and Newell, 1967; Bers, 1975; Kaup, 1979; Chow, 1991). We studied the dynamics of a nonconservative 3WI in one spatial dimension x and time t. For weakly growing and damped waves this 3WI has the form (Chow, 1991; Chow *et al.*, 1992a)

$$\partial_t a_i - D\partial_{xx} a_i - \gamma_i a_i = -a_j a_k \tag{1}$$

$$\partial_t a_j + v_j \partial_x a_j + \gamma_j a_j = a_i a_k^* \tag{2}$$

$$\partial_t a_k + v_k \partial_x a_k + \gamma_k a_k = a_i a_j^*, \tag{3}$$

where the a's are complex wave envelopes, the γ's are growth or damping coefficients, v's are group velocities (the interaction is described in the frame of the wave packets), the nonlinear coupling is taken as unity and D is a diffusion coefficient. The diffusion term is usually not included in the 3WI.

This term arises if we assume that the growth of the linear wave has a slow spatial variation. It is then the lowest order reflection invariant term that provides a cutoff in wave number of the growth. Without this term the problem is not well posed. It will become apparent later that this term is essential for nonlinear saturation and is very important in determining the long time behavior.[1] The subscript i denotes the high frequency unstable parent wave. The other two waves are referred to as the daughters. We will consider the case where the daughter waves have equal damping (i.e. $\gamma_j = \gamma_k$). The length and time can then be rescaled so that the damping coefficient is unity.

The order of the group velocities determines the behavior of the conservative ($\gamma = D = 0$) nonlinear interactions (Kaup *et al.*, 1979). If the high frequency wave has the middle group velocity then solitons are transferred from the parent to the daughter waves. This case is known as the soliton decay interaction (SDI). As an example, this situation may occur in the decay of lower hybrid waves. This also corresponds to the nonlinear saturation of an absolute parametric instability in the parent wave frame. If the parent wave has the highest or lowest group velocity then soliton exchange is no longer possible and the collisions between wave packets become important. This case is physically most common. It is the nonlinear saturation of a convective parametric instability in the parent frame. This situation applies for example to the Langmuir decay interaction (LDI) and may have implications in the saturation of stimulated Raman scattering (SRS) observed in intense laser-plasma interactions (Batha *et al.*, 1991). In the nonconservative nonlinear interaction described by (1)-(3) both SDI and LDI exhibit STC. The first is described in Section 2 and the second in Section 3.

SOLITON DECAY INTERACTION

For SDI the group velocities satisfy the condition $v_k > 0 > v_j$ (i.e., the highest frequency parent wave has the middle group velocity[2]). In the absence of growth, damping and diffusion ($\gamma_i = D = 0$) the IST solutions for this group velocity ordering is described by soliton exchange between wavepackets (Kaup *et al.*, 1979; Kaup, 1976a; Bers *et al.*, 1976).

We numerically simulated the system Eqs. (1)-(3) on the domain $x \in [0, L)$ with periodic boundary conditions. We began with random real initial conditions and evolved until the transients died away before the system was analyzed. It can be shown that for real valued intitial conditions the envelopes remain real for all time (Kaup *et al.*, 1979; Chow, 1991). We were interested in the large system, long time limit. We considered the case with parameters $D = 0.001$, $\gamma_i = 0.1$, $\gamma_j = \gamma_k = 1$, and $L = 20$. These parameters were chosen because they exhibit STC and fall into a regime where the results can be understood by perturbation theory on the conservative solution. However, the system is extremely rich and different parameters do lead to vastly different behavior. Aspects of these different regimes will be touched upon later and details are given in (Chow, 1991). We measured the correlation function, $S_l(x,t) =< a_l(x-x', t-t')a_l(x',t') >$, where the angled brackets denote spacetime averages.

A sample of the spatiotemporal evolution profiles in the STC regime of the parent and daughter envelopes is given in Fig. 1. The length shown is one half the system size and $t = 0$ is an arbitrary time well after the transients have decayed. The profile of the parent wave is irregular but spatial and temporal scales can be observed. There are coherent structures of a definite length scale that can be seen to grow, deplete and collide with one another. The profile of the daughter wave shows a sea of structures convecting to the left. We only show one daughter, the other will be similar but with structures convecting to the right. Figure 2 shows the spectrum of static fluctuations $S_l(t = 0, q)$. For the parent wave there is a cutoff near $q \simeq 10$ and a range of modes show up as

[1] An equivalent set of 3WI equations can be written in two spatial dimensions (e.g. x and y) for nonlinear interactions in the steady state (Kaup *et al.*, 1979); the equations are of the same form where t is y and, in each equation, all other terms are divided by the y-component of the group velocity of the wave. Thus the solutions we describe (x,t) apply also to (x,y) with appropriate boundary conditions.

[2] In the two-dimensional steady-state, see (Kaup *et al.*, 1979) and (Benney and Newell, 1967), this condition involves only the ratios of group velocity components.

a prominent hump. The cutoff reflects the length scale seen in the spacetime profile. For q below the hump the spectrum is flat. The daughter spectrum has a cutoff around $q \simeq 6$ again indicating a length scale. Figure 3 shows the local power spectrum $S_l(\omega, x = 0)$. The spectrum for the parent clearly shows two time scales. The spectrum bends over near $\omega \simeq 0.02$ which gives a long time scale and a shoulder at $\omega \simeq 0.3$ gives a short time scale. The short time scale appears as the growth and depletion cycle observed in the spatiotemporal profile. The daughter power spectrum has two peaks at high ω. One is where the shoulder of the parent spectrum is and the other is at twice this frequency. The spectrum begins to bend over and flatten out at at $\omega \simeq 0.007$.

The main features of the behavior can be understood if we consider the growth and dissipation as perturbations about the conservative 3WI. The IST solutions for the conservative case on the infinite domain show that solitons exist but they do not necessarily belong uniquely to a particular envelope. Solitons in the parent wave tend to deplete to solitons in the daughters which propagate away. The simplest soliton solution for decay shows that a soliton of the form $|a_i| = 2\eta \mathrm{sech} 2\eta x$, will decay into solitons in the daughters of the form $|a_j| = \sqrt{2}\eta \mathrm{sech}\eta(x + v_j t)$, where η is the IST spectral parameter for the Zakharov-Manakov (Zakharov and Manakov, 1973) scattering problem. The spectral parameter is also the eigenvalue for a bound state in the Zakharov-Shabat (Zakharov and Shabat, 1971) scattering problem with the parent pulse as the potential function. In the WKB limit η is related to the area of the parent pulse through the Bohr quantization condition

$$\int_a^b |a_i^2 - \eta^2|^{1/2} dx = \pi/2, \tag{4}$$

where $[a, b]$ are turning points for a local pulse. A collision between a daughter pulse and a parent soliton is necessary to induce the decay of the parent (Bers *et al.*, 1976; Kaup *et al.*, 1979). For arbitrary shaped parent pulses that exceed the area threshold, the soliton content will be transferred to the daughters leaving the radiation behind in the parent pulse. Collisions between daughter solitons are elastic.

With the addition of weak growth and dissipation, parent pulses deplete provided they satisfy the WKB threshold condition (Chow *et al.*, 1992a; Bers, 1983).

$$\int_a^b |a_i^2 - \gamma_j^2|^{1/2} dx > \pi/2. \tag{5}$$

The decay products in the daughters are quasi-solitons; they damp as they propagate away and do not collide elastically. The soliton content of the parent is not completely transferred to the daughters. The parent wave with some initial local eigenvalue η will deplete and be left with some remaining area. This area is due to the conversion of soliton content into radiation by the perturbations. This left over area can be represented by an effective 'eigenvalue' η'. This remaining part of the parent will then grow until it exceeds the threshold for decay. This time denoted by t_c is given by

$$t_c \simeq \frac{1}{\gamma_i} \ln \frac{\eta}{\eta'}. \tag{6}$$

The cycling time observed in the spacetime profiles is this time plus the time required to deplete. The depletion time from IST theory is on the order $1/2\eta$ and for $\gamma_i \ll 2\eta$ this can be neglected and t_c gives the cycling time. By treating the damping and growth as a slow time scale perturbation of the IST soliton decay solution described above and ignoring the effects of diffusion on this short time scale, a multiple-time scale perturbation analysis about the IST soliton solution was used to estimate η'. In this calculation the ordering $\gamma_i \ll \gamma_j \ll 2\eta$ was chosen. The small parameter is $\gamma_j/2\eta$ but by simply rescaling in time and space either γ_j or η can be scaled to $O(1)$. To leading order this yields (Chow, 1991)

$$\eta' \simeq \gamma_j. \tag{7}$$

The derivation assumes that the depletion time for a soliton is very much faster than the growth and damping time. Simulations for parent soliton initial conditions verify Eq. (7) (Chow, 1991). In order to complete the calculation for the cycling time t_c, it is necessary to estimate the threshold local η required for decay. By comparing the Bohr quantization condition (4) with the WKB condition for

decay with damping (5) we know that $\eta > \gamma_j$. Using the IST scattering space perturbation theory developed by Kaup (Kaup *et al.*, 1979; Kaup, 1976b; Kaup and Newell, 1978) and recently reviewed in Kivshar and Malomed (1989), we constructed the time dependence of the IST scattering data due to the perturbation. The same ordering as the multiple scale calculation was chosen. From this we were able to estimate η to leading order to be (Chow, 1991)

$$\eta \simeq 2\gamma_j + 4\xi_p\gamma_i, \tag{8}$$

where ξ_p is the parent correlation length and will be defined later. Equation (8) is sensitive to the amplitudes of the colliding daughter waves that induce the decay. The calculation assumes the decay is induced by collisions with quasi-solitons with the same phase from each daughter generated two correlation lengths away. The relative phases of the colliding daughters is very important. Consider real amplitudes for the moment, Eq. (1) shows that two daughter quasi-solitons with opposite signs (phase) actually reinforce the parent rather than make it deplete. Because of other effects, expression (8) should be considered more of a lower bound. In the simulation, radiation and diffusive effects will be relevant and may also further delay the decay of the parent. From η we are able to estimate the daughter correlation length. This is given by the quasi-soliton width $\xi_d \simeq 2/\eta$.

The long time behavior is governed by the diffusion. The trivial fixed point of Eq. (1) is given by

$$\partial_{xx}a_i + q_0^2 a_i = 0, \qquad a_j = a_k = 0, \tag{9}$$

where $q_0 = \sqrt{\gamma_i/D}$. Modes with $q > q_0$ will damp and those with $q < q_0$ will grow. Thus the fixed point is always unstable to long wave length fluctuations. However, when a local area between two turning points of the parent wave contains a bound state with eigenvalue η it will deplete. In the depletion process broad parent pulses will be decimated. The growth in the $q < q_0$ modes are thus saturated nonlinearly. This results in long wavelength distortions beyond lengths $2\pi/q_0$. The principal mode q_0 was observed as the cutoff in the spectrum of static fluctuations (Fig. 2a). The mode q_0 defines the correlation length for the parent, $\xi_p \simeq 2\pi/q_0$. If $D = 0$ there will not be any nonlinear saturation of the instability because q_0 would become infinite and so would the amplitude required to fulfill the area threshold (5).

The long time scale for the parent τ_p is given by the diffusion time across a length ξ_p giving $\tau_p \simeq (2\pi)^2/\gamma_i$. This is the time scale in which the local parent structures will shift position, collide with other structures or diffuse away. The long correlation time observed in the daughters is associated with the interaction of the daughter quasi-solitons with the parent structures. Whenever quasi-solitons collide with the parent structures they may induce a decay and create a new quasi-soliton where the collision occurred. This would lead to a long correlation time for the daughters. As the parent structures drift so would the creation location of new quasi-solitons. However because the quasi-solitons have a larger width than the parent structures, the long time scale for the daughters would be given by the diffusion time across a quasi-soliton width yielding $\tau_d \simeq 4/(\eta^2 D)$. The newly created quasi-soliton damps while it continues to propagate along the characteristic. However when it collides with another parent structure it could induce a decay and repeat the process. The parent structures act as amplifiers regenerating damped quasi-solitons that collide with them.

Using the above analysis for the parameters of the simulation we obtain the following estimates: $\tau_p \simeq 400$, $q_0 = 10$, $\xi_p \simeq 0.6$, $\eta' \simeq 1$, $\eta \simeq 2.2$, $t_c \simeq 8$, $\xi_d \simeq 0.9$, $\tau_d \simeq 800$. These estimates corroborate fairly well with the simulation. The estimate for t_c is a bit low compared to the shoulder in the parent power spectra at $\omega \sim 0.3$ corresponding to $t \simeq 20$. This is because many effects due to radiation, diffusion and strong overlap of the envelopes were not accounted for. However the spacetime profiles in Fig. 1 do show some of the parent structures cycling near the predicted time scale, so the calculation does predict a lower bound.

A word should be said about the system size. It is clear with the very long correlation times for the daughters that they cycle the box many times before correlations decay away. Thus for long times, the temporal correlation function along the characteristic or at a single spatial location would be the same. This was born out in the simulation. It is unknown what the precise boundary effects

are since it would be impossible to numerically test a system large compared to this long time scale. However with other runs of varying length, it was found that the above time scales seem to be unaffected by the box size as long as the box is much larger than ξ_p. The power law rise for the parent power spectrum below $2\pi/\tau_p$, seems to decrease in exponent as the system increases.

We chose parameters where perturbation theory about the IST solutions could be applied to try to understand the dynamics. However the behavior does dramatically change for different parameter regimes (Chow, 1991). For growth rates not small compared to the damping rates, the long time scales observed tend to disappear and only the growth and depletion cycling time is evident. The parent grows strongly and depletes violently preventing the structures to become established. The larger the growth rate the larger the amplitudes of the quasi-solitons (Chow, 1991). Another regime is when the diffusion is comparable to the damping so the parent structures are much broader than the damping length of the daughters. In this situation the daughters grow and damp within the confines of a parent pulse. Spatial exchange of information between these pulses is very slow. These and other regimes are reported in Chow (1991).

LANGMUIR DECAY INTERACTION

In LDI the group velocities satisfy, without loss of generality, $v_k < v_j < 0$. For the simulation the values $v_j = -1, v_k = -2$ were chosen. Using laser plasma terminology, wave a_i is referred to as the pump wave (PW), wave a_j is the acoustic wave (AW) and wave a_k is the backscattered wave (BW). The Eqs. (1)-(3) were simulated on the domain $x \in [0, L)$ with periodic boundary conditions. The long time, large system limit was of interest. Simulations were started with random real initial conditions. As in the SDI case the envelopes remain real for all time. The spacetime history was recorded for all the envelopes. In the saturated regime the correlation functions $S_i(x,t) =< a_i(x-x', t-t')a_i(x',t')$ were computed. As in SDI the parameter set is given by (D, γ_i).

Several different parameter sets were used in the simulations. In the first example the parameters were: $\gamma_i = 0.1$, $D = 0.004$ and $L = 20$. As will be seen later the length plays an important role in the dynamics. The spatiotemporal profile of the PW is shown in Fig. 4a. Again furrowed, ridgelike 'coherent' structures are observed, as in the SDI but with a definite drift towards the right. There appear to be length and time scales where things are correlated, but beyond which the dynamics becomes chaotic. The correlation function for the PW is shown in Fig. 4b. The function approaches zero in space and time indicating STC but a nonlinearly induced mode with a definite phase velocity is clearly observed. This effect was observed in the spacetime profiles as the drifting coherent structures. The correlation function shows that these structures are very long lived.

The local power spectrum $S_i(x = 0, \omega)$ is shown in Fig. 5a. A definite peak at $\omega \simeq .1$ is observed; the spectrum then flattens out at around $\omega \simeq 0.007$ defining a correlation time. The spectrum of static fluctuations $S_i(q, t = 0)$ is shown in Fig. 5b. A box-like function, as expected, is observed with a cutoff at approximately $q \simeq 5$, translating to a correlation length of $\xi_p \simeq 1.3$.

The spacetime profile of the AW is shown in Fig. 6a. Ridgelike coherent structures are seen to drift towards the left. For large scales the dynamics are chaotic. The correlation function measured along the characteristic $x = -t$ is given in Fig. 6b. There is strong decay in space and time confirming STC. However there is a hump located at $S(x \simeq 10, t \simeq 10)$, and another at $S(x \simeq 1, t \simeq 20)$. The latter is due to the collision of the AW coherent structure after one transit around the box. Because the PW is drifting the bump is located away from $x = 0$. The former bump comes from the interaction of the BW with the PW generating the AW. Since the BW travels at twice the AW velocity this event occurs at half the time the AW requires to traverse the box. Note that the correlation function shown is over the entire length of the system, and the periodicity of the system is seen for $t = 0$. The power spectrum is shown in Fig. 7a. The correlation time corresponds to a frequency of $\omega \simeq 0.3$. The spectrum of static fluctuations is shown in Fig. 7b. There is a cutoff at $q \simeq 9$ corresponding to a correlation length of $\xi_a \simeq 0.7$.

The spacetime profile of the BW is shown in Fig. 8a. Again irregular yet distinct structures are seen to drift towards the left. The correlation function measured along the characteristic $x = -2t$ is shown in Fig. 8b. Correlations approach zero in space and time indicating STC. A nonlinear mode similar to the parent is also observed. The propagating mode implies that the structures found in Fig. 8a are not aligned along the characteristic curve but are actually moving faster. The measured phase velocity in the moving frame $v \simeq 0.1$ indicates that the shift away from the characteristic velocity is not very great. Correlations in the direction of the coherent structures are fairly long compared to the damping times. The power spectrum along the characteristic in Fig. 9a shows a cutoff around $\omega \simeq 0.4$. The spectrum of static fluctuations in Fig. 9b shows a cutoff around $q \simeq 5$ giving a correlation length of $\xi_b \simeq 1.3$.

The simulation results can be understood with the aid of linear analysis and the IST solutions. The linearized equation for the PW is exactly the same as that for the parent wave in SDI. The trivial fixed point Eq. (9) gives a principal mode for the PW at $q_0 = \sqrt{\gamma_i/D}$. Higher modes are damped and lower modes are growing. As in SDI there is a competition between linear growth and nonlinear saturation. Instead of depletion to quasi-solitons seen in SDI, the saturation mechanism is due to the collisions between the envelopes. The balance between the competing effects is also responsible for the propagating mode as will be shown.

The IST solutions which apply to the conservative form of LDI show solitons are not involved (Kaup *et al.*, 1979). The interesting dynamics are due to collisional radiation effects. A collision between the AW and the PW generates the BW and decimates all the waves (Kaup *et al.*, 1979; Chow, 1991). Similar behavior occurs when the BW collides with the PW. The decimation of the parent wave is always on the side opposite to that of the collision. This is seen in the IST solutions and can be understood from the nonlinear saturation of the corresponding parametric instability. When the AW collides with the PW, the BW and AW grow from the colliding edge as a convective instability. This is because both of their group velocities are in the same direction. When the two envelopes attain a significant amplitude the PW begins to saturate. However the two daughter waves will continue to grow and continue to take energy from the PW. The energy of the PW will be reduced. The depleting pump cuts off the growth of the two daughter waves and they saturate and begin to damp as well. If the original amplitude of the PW is large enough or the growth rate γ_i high enough, the reduction in area continues until the PW becomes negative. The negative part of the PW can again be a source for a convective instability and the same process ensues. In this way the envelopes are spatially decimated into the oscillatory structures seen in the simulation. The decimation is always on the side of the PW away from the colliding edge. The low q's are converted to high q's by this process. Modes higher than q_0 get damped, so the PW will settle into structures of size $\xi_p \simeq 2\pi/q_0$. The values $q_0 = 5$ and $\xi_p \simeq 1.3$, obtained for the simulation parameter set, agree well with the simulation.

The PW equation Eq. (1) has the form of a growing diffusion equation. Thus any localized pulse will spread and grow. The propagating PW mode is a result of the combination of this spreading effect and the decimation effect. The wavepackets decimate nonlinearly on one side and they spread and grow linearly on the other side. A pulse moves like a sandbar near an ocean shore, building on one side and receding on the other. A parabolic equation does not have a well defined phase velocity, but a 'spreading' velocity can be defined by considering the trajectory of a point of constant amplitude on a localized pulse. The phase velocity of the sandbar mode, as it will be referred to, will then be given by this velocity which can be shown to be proportional to $\sqrt{D\gamma_i}$ (Chow, 1991). From the simulations of several different cases it was discovered that the phase velocity behaves as $v_p \simeq \sqrt{D\gamma_i}$.

The peak in the PW power spectrum is given by the frequency of the sandbar mode. Using the relation $\omega = v_p q_0$ the frequency is found to be $\omega \simeq \gamma_i = .1$. This is precisely what was observed in Fig. 5a. As seen in the correlation function in Fig. 4b, the structures remain coherent for very long times. The power spectrum in Fig. 5a was taken along the time axis. The long time scale

observed was actually given by the transit time of the sandbar mode around the box $\tau_P \simeq L/v_p$. It is unknown what the decorrelation mechanism for the PW coherent structures actually is. They persist much longer than the diffusion time across a correlation length.

The saturation energy of the PW can be understood as follows. The competition between the nonlinear and linear effects leads to coherent structures of size $2\pi/q_0$. The IST solutions show for the conservative case that structures of this size are generated in collisions when the PW has a height of $a_i \simeq q_0$. For taller structures, the collisions with the BW and AW will generate structures with smaller wavelengths. The simulations seemed to indicate that these results of the integrable case carry over to the nonintegrable regime. Then as the PW grows, it gets depleted as it constantly collides with the other waves. If it grows higher than $a_i \simeq q_0$ the generated structures damp away. Thus $a_i \simeq q_0$ will be an upper bound to the height of the PW. For these parameters $q_0 \simeq 5$ and the tallest structures in the spacetime profile are of this order. Given the upper bound for the PW height, the saturated energy density can be estimated by considering the PW to be composed of coherent structures locally resembling a sine wave with average amplitude of $q_0/2$. This then gives an average energy density of $S_i(0,0) \simeq q_0^2/4 \simeq 6$. The simulation shows a value of $S_i(0,0) \simeq 5$. Considering the assumptions used in the estimate this is remarkably good.

It is significant that the correlation length for the AW is one half the correlation length of the BW. This is due to the fact that its group velocity is half of the BW. As discussed above the PW settles into coherent structures of size ξ_p, and this fixes the size of the BW structures. The AW gets generated wherever the BW collides with the PW. In the time direction, along a PW coherent structure, the BW and AW will tend to have the same number of coherent structures. This can be seen by comparing Fig. 6a with Fig. 8a. However since the AW has a group velocity half that of the BW, if it has the same number of structures in the time direction, it must have twice as many in the spatial direction. In other words the coherent structures of the AW are half the size of the BW. This was observed in the simulation. In the saturated state, a lattice-like structure will become established. Of course it is only for special cases that a regular lattice can be formed. In most cases the lattice will be frustrated. This leads to the lack of regularity and STC observed. It would be very useful in the future to measure the cross correlation function between the waves to better understand these effects.

The propagating mode of the BW seen in the correlation function can also be inferred from the IST solution. The correlation function showed that the propagation velocity of the coherent structures was slightly slower than the characteristic velocity. During a collision between the BW with the PW, the two waves will interact nonlinearly and this process retards the transmission of the BW, slowing the velocity.

The AW spacetime profile in Fig. 6a shows a furrowed structure moving to the left like the BW, but the correlation function in Fig. 8a does not show the long correlations and evidence of a nonlinear mode like the BW and PW. Correlations are quickly damped out compared to the other waves. This is likely due in part to the fact that since the group velocity is half that of the BW, it experiences twice as much damping between collisions. It may also be that the wave collisions affect the AW more than the other waves. The humps observed in the AW correlation function are due to collisions of the AW with the PW and BW waves. The one at $(x \simeq 1, t \simeq 20)$, is due to repeated collisions of the AW with a particular PW structure. The correlation times of the PW structures are very long. Each time the AW circles the simulation box it will collide with the PW structure. The hump is slightly off from the characteristic. This is due to the fact that the PW structure is drifting. The hump at $(x \simeq 10, t \simeq 10)$ is due to collisions between a given BW structure and the PW structure. Whenever these two waves collide they generate the AW in the process. The BW has group velocity twice that of the AW and so transits the box in a time $t = 10$. In the frame of the AW the hump gets shifted in x as well.

It would seem that the behavior observed for LDI should persist as the PW growth rate increases or the diffusion decreases. The PW structures would reduce in width and this would lead to an increase in their amplitude. The ratio of the PW energy to the daughters would approach unity. However in the weak growth limit the ratio of the PW energy to the daughter energies would be large. The PW structures would become wider and their amplitudes smaller. The daughter waves would damp more between collisions. The coherence times would likely become longer as in the SDI case. The energies of the daughter waves would also get smaller in comparison to the PW's and the nonlinearity would become less important. Differences in the ratios of the velocity would change the ratio of the sizes of the AW and BW. Differences in the damping rates on the daughters would change the saturation energies. If the disparity were large than the wave with the lower damping would dominate the nonlinear collision processes. These effects were seen in preliminary simulations. A detailed analysis remains to be done.

The spectral broadening and amplitude saturation of the unstable wave occurs for almost all parameters. As an application we have considered the saturation of SRS due to decay of the electron plasma wave (epw) (Chow, 1991). The unstable epw in SRS can decay rapidly to another epw and ion-acoustic wave. The ensuing STC broadens the spectrum and saturates this epw which, for a fixed input laser power, leads to the saturation of the scattered wave in SRS. Further details will be given in an upcoming publication.

One of us (C.C.) wishes to thank T. Hwa and D. Kaup for fruitful and interesting discussions. This work was supported in part by NSF Grant No. ECS-88-2475, LLNL subcontract B160456, DOE Grant No. DE-FG02-91ER-54109, and NASA Grant No. NAGW-2048.

REFERENCES

Arrechi, F. T., G. Giacomelli, P. L. Ramazza, and S. Residori (1990). *Phys. Rev. Lett.*, 65, 2531.

Batha, S. H., D. S. Montgomery, K. S. Bradley, R. P. Drake, K. Estabrook, and B. A. Remington (1991). *Phys. Rev. Lett.*, 66, 2324.

Benney D. J. and A. C. Newell (1967). *J. Math. Phys.*, 46, 133.

Bers, A. (1975). In: *Plasma Physics-Les Houches 1972*, eds. C. De Witt and J. Peyraud (Gordon and Breach, New York).

Bers, A. (1983). In: *Handbook of Plasma Physics*, eds. M. N. Rosenbluth and R. Z. Sagdeev (North Holland, Amsterdam, 1983), Vol. 1, Chap. 3.2.

Bers, A., D. J. Kaup, and A. H. Reiman (1976). *Phys. Rev. Lett.*, 37, 182.

Chow, C. C. (1991). Ph.D. Thesis, Department of Physics, Massachusetts Institute of Technology, Cambridge, Mass., USA.

Chow, C. C., A. Bers, and A. K. Ram (1992). in *Research Trends in Physics: Chaotic Dynamics and Transport in Fluids and Plasmas* eds. I. Prigogine *et al.* (American Institute of Physics, New York).

Chow, C. C., A. Bers, and A. K. Ram (1992). *Phys. Rev. Lett.*, 68, 3379.

Ciliberto, S. and M. Caponeri (1990). *Phys. Rev. Lett.*, 64, 2775.

Coullet, P., C. Elphick, and D. Repaux (1987). *Phys. Rev. Lett.*, 58, 431.

Hohenberg, P. C. and B. I. Shraiman (1989). *Physica D*, 37, 109 and references therein.

Kaup, D. J. (1976). *Stud. Appl. Math.*, 55, 9.

Kaup, D. J. (1976). *SIAM J. Appl. Math.*, 31, 121.

Kaup, D. J., A. Reiman, and A. Bers (1979). *Rev. Mod. Phys.*, 51, 915 and references therein.

Kaup, D. J. and A. C. Newell (1978). *Proc. R. Soc. Lond. A.*, 361, 413.

Kivshar, Y. S. and B. A. Malomed (1989). *Rev. Mod. Phys.*, 61, 763.

Remington, B. A. (1991). *Phys. Rev. Lett.*, 66, 2324.

Zakharov, V. E. and S. V. Manakov (1973). *Zh. Eksp. Teor. Fiz. Pis'ma Red.* 18, 413 [*Sov. Phys.,—JETP Lett.*, 18, 243].

Zakharov, V. E. and A. B. Shabat (1971). *Zh. Eksp. Teor. Fiz.*, 61, 118 [*Sov. Phys.,—JETP* 34, 62].

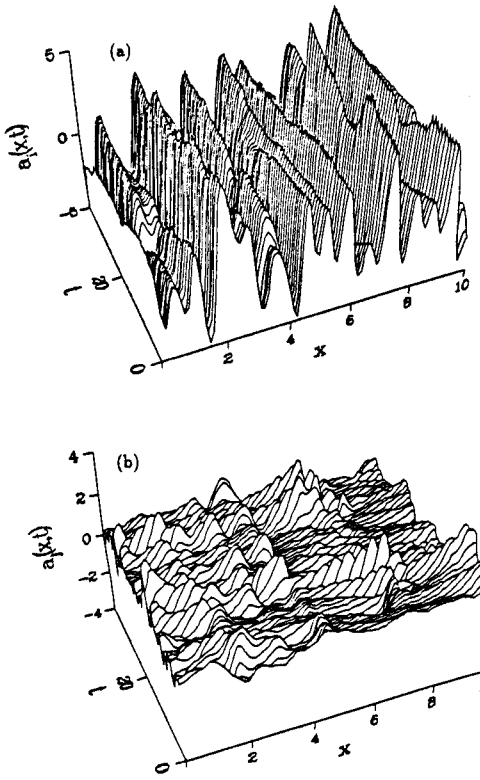

Fig. 1. Spatiotemporal profiles of the parent wave a) and daughter wave b) for SDI.

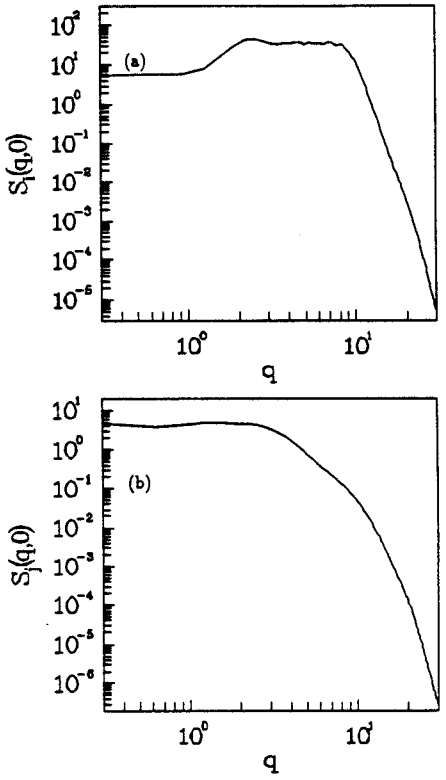

Fig. 2. Spectrum of static fluctuations $S_l(q,t = 0)$ of the parent wave a) and daughter wave b) for SDI.

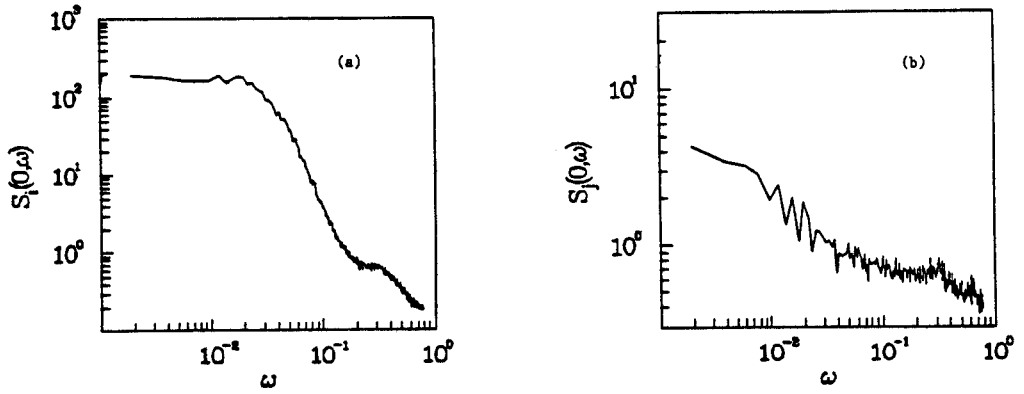

Fig. 3. Local power spectrum $S_l(x = 0, \omega)$ of the parent wave a) and daughter wave b) for SDI.

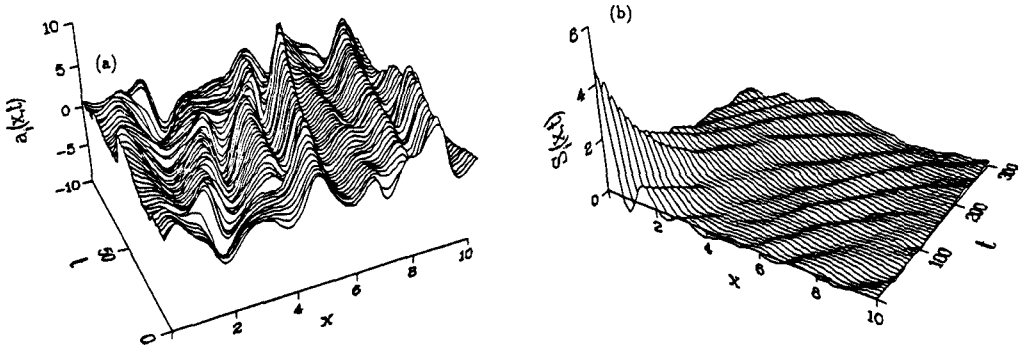

Fig. 4. Spatiotemporal profile a) and correlation function b) of the PW for LDI.

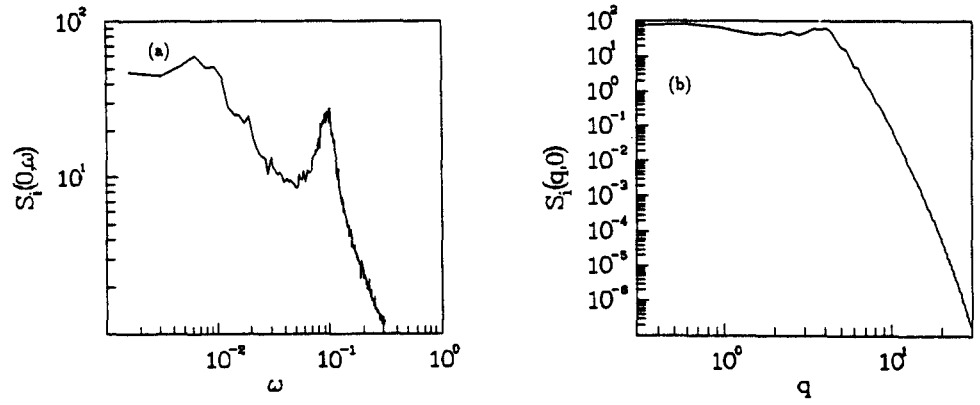

Fig. 5. Local power spectrum a) and spectrum of static fluctuations b) for the PW for LDI.

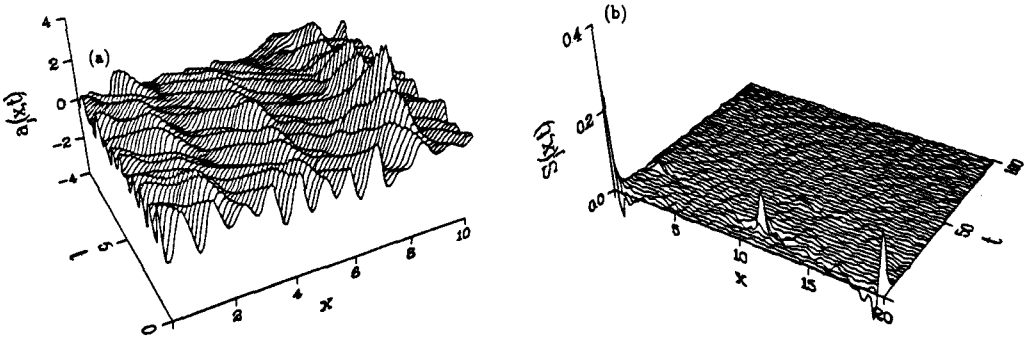

Fig. 6. Spatiotemporal profile a) and correlation function b) of the AW for LDI.

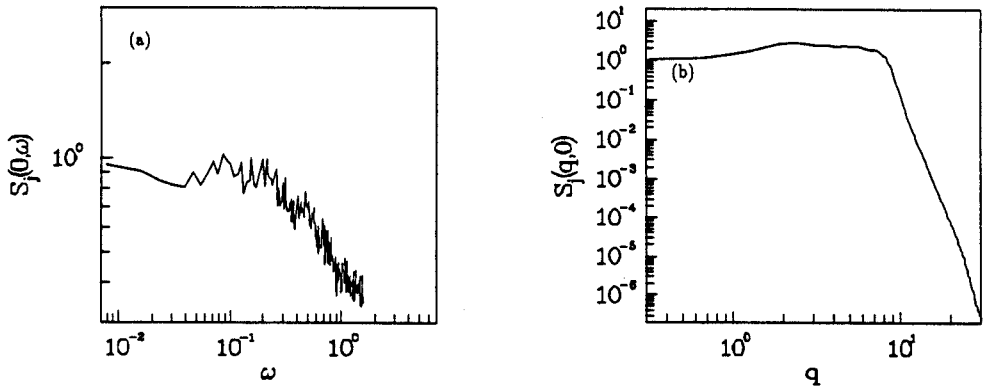

Fig. 7. Local power spectrum a) and spectrum of static fluctuations b) for the AW for LDI.

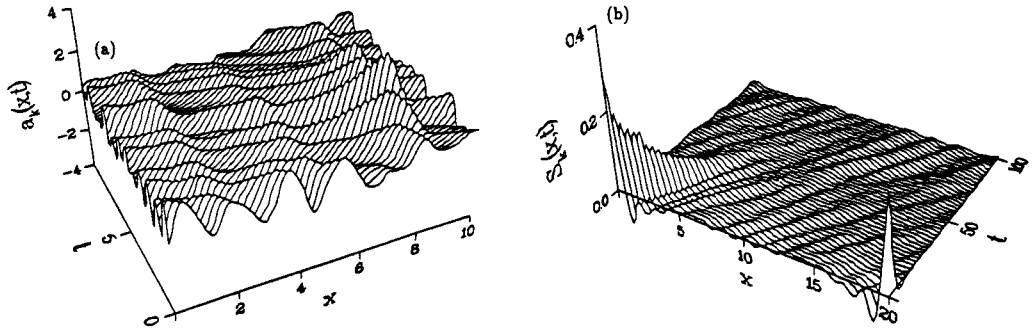

Fig. 8. Spatiotemporal profile a) and correlation function b) of the BW for LDI.

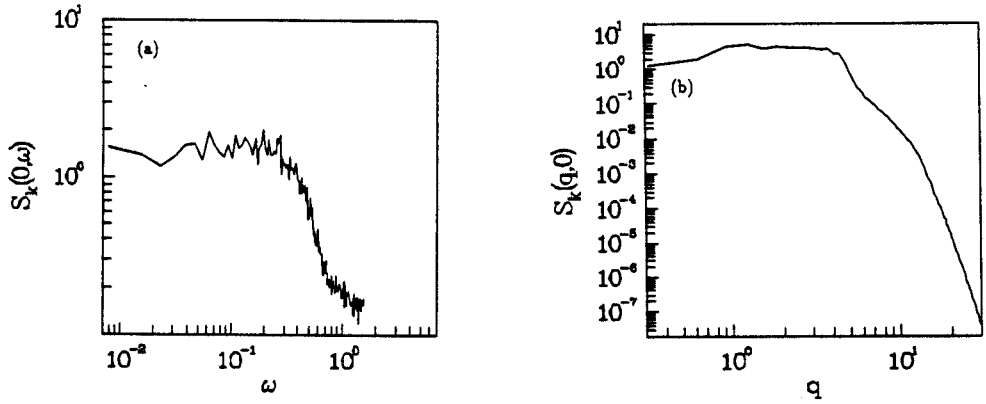

Fig. 9. Local power spectrum a) and spectrum of static fluctuations b) for the BW for LDI.